

# Duck-curve Mitigation in Power Grids with High Penetration of PV Generation

Ivan Calero, *Member, IEEE*, Claudio A. Cañizares, *Fellow, IEEE*, Kankar Bhattacharya, *Fellow, IEEE*, and Ross Baldick, *Fellow, IEEE*

**Abstract**—Small-scale PV generation has become popular with residential customers in several jurisdictions with high solar radiation, as an alternative to improve their carbon footprint and reduce their electricity bills. However, massive deployment of such distributed generation is creating a particular and undesirable shape in the net demand, which deepens at hours of peak solar PV injections at noon and suddenly rises towards the evening, known as the “duck curve”. Hence, this paper investigates the use of pre-cooling strategies in residential households to mitigate the duck-curve effects. To this aim, appropriate thermal models and simulations of houses are first developed and carried out to demonstrate the technical feasibility of pre-cooling in a house with a typical configuration, based on the Smart Residential Load Simulator (SRLS) developed at the University of Waterloo. Then, an aggregation technique is proposed to evaluate the effects on a large grid of different penetration levels of PV, and pre-cooling approaches to manage the duck-curve in California and Texas, concluding that such techniques are capable of substantially flattening the system net demand curve.

**Index Terms**—Demand response, duck curve, house thermal modeling, pre-cooling, PV, thermal mass.

## NOMENCLATURE

### Indices

$b$	Base demand
$H$	Hour index
$i, j$	Room indices
$k$	Index of data points in average profiles
$l$	Index of randomly generated households with pre-cooling load profiles
$m$	Wall orientation index
max	Maximum
$o$	High-resolution detailed household profiles
$pc$	Index of randomly generated households
$PV$	PV generation
$r$	Residential demand
$s$	Index of randomly generated households with BAU load profiles
$u$	Wall/window layer index

### Parameters

$C_f$	Thermal capacitance of room’s floor [K/J]
$C_{in}$	Thermal capacitance of room, excluding walls and floor [K/J]
$c_p$	Specific heat capacity [J/K.kg]
$C_w$	Thermal capacitance of walls [K/J]
$h_i$	Room’s $i$ height [m]
$\mathcal{K}$	Thermal conductivity [W/m.K]
$L$	Number of random households with pre-cooling
$l_i$	Room’s $i$ length [m]
$M$	Number of data points in the interval $\Delta t$
$N$	Number of data points in average profiles
$PV_{sys}$	Total residential PV generation [kW]
$R_c$	Thermal resistance of windows [K/W]
$R_f$	Thermal resistance of room’s floor [K/W]
$R_w$	Thermal resistance of walls [K/W]
$S$	Number of random BAU household load profiles
$SHGC$	Solar heat gain coefficient
$T_g$	Ground temperature [K]
$U$	Number of layers in windows/walls
$w_i$	Room’s $i$ width [m]
$x$	Wall/window layer thickness [m]
$\beta$	Fraction of households with pre-cooling
$\Delta t$	Time resolution [h]
$\kappa$	Absortance
$\mu_i$	Distribution heat factor of room $i$
$\rho$	Density [kg/m <sup>3</sup> ]
$\tau$	Transmittance
$\phi$	Latitude [deg]
$\Omega$	Fraction of room volume occupied by furniture

### Variables

$\mathbf{A}$	Wall matrix [m <sup>2</sup> ]
$a, b, \zeta$	Auxiliary variables
$\mathcal{B}$	Sky brightness
$B_{i,j}$	Internal wall area shared by rooms $i$ and $j$ [m <sup>2</sup> ]
$\mathbf{D}$	Aggregated demand vector
$\mathbf{d}$	Vector containing the household load profile for BAU case [kW]
$E_{i,m}$	Wall area of room $i$ facing the direction $m$ [m <sup>2</sup> ]
$\mathbf{f}$	Vector containing the household load profile for pre-cooling case [kW]
$F_1$	Circumsolar brightness coefficient
$F_2$	Horizon brightness coefficient

The work presented in this paper has been funded by NSERC and the University of Waterloo.

I. Calero, C. Cañizares, and K. Bhattacharya are with the Department of Electrical and Computer Engineering, University of Waterloo, Waterloo, ON, N2L 3G1, Canada (e-mail: icalero@uwaterloo.ca; ccanizar@uwaterloo.ca; kankar@uwaterloo.ca).

R. Baldick is with the Department of Electrical and Computer Engineering, University of Texas at Austin, Austin, TX 78751 USA (e-mail: baldick@ece.utexas.edu).

$G$	Aggregated PV generation
$g$	Vector containing the household PV generation profile [kW]
$H_o$	Total households in the system
$I_b$	Beam solar irradiance [W/m <sup>2</sup> ]
$I_h$	Horizontal diffuse solar irradiance [W/m <sup>2</sup> ]
$I_m$	Total solar irradiance incident to external wall facing direction $m$ [W/m <sup>2</sup> ]
$J_{err}$	Objective function accounting for the accuracy of the model prediction
$J_{var}$	Objective function accounting for the smoothness of the load profile
$O_{i,m}$	External wall area of room $i$ facing the direction $m$ [m <sup>2</sup> ]
$P$	Probability matrix
$Q_c$	Solar heating power onto windows [W]
$Q_{in}$	Heating power from active people in the house [W]
$Q_{HVAC}$	Heating power of central HVAC system [W]
$Q_{pl}$	Heating power per active people [W]
$Q_{sr}$	Solar heating power onto external walls [W]
$t$	Time vector associated with average load profiles [h]
$t_H$	Day time [h]
$T_{am}$	Ambient temperature [K]
$T_f$	Floor temperature [K]
$T_{in}$	Room temperature [K]
$T_w$	Wall temperature [K]
$\mathcal{T}$	Time-associated random variable [h]
$V$	Topology matrix
$W_{i,m}$	Total area of windows in room $i$ facing the direction $m$ [m <sup>2</sup> ]
$Z_{pc}$	Probability matrix associated with a random load profile $pc$
$\alpha$	Fraction of houses with PV systems
$\gamma$	Azimuth angle [deg]
$\delta$	Declination angle [deg]
$\epsilon$	Fraction of households with demand $\bar{d}$
$\zeta$	Solar altitude angle [deg]
$\theta_m$	Incidence angle to the external walls in the direction $m$ [deg]
$\vartheta$	Hemispherical ground reflectance
$\lambda_k$	Fraction of system demand that corresponds to base load, at time $t_k$
$\Sigma$	Vector of standard deviations [h]
$\sigma$	Standard deviation [h]
$\xi_t$	Number of active people in the house at time $t$
$\psi$	Inclination angle [deg]
$\omega$	Hour angle [deg]
$\sim$	Average variables
$\hat{\phantom{x}}$	Estimated values
$\bar{\phantom{x}}$	Expected values

## I. INTRODUCTION

According to the International Energy Outlook [1], by 2050, renewables will account for almost half of the

world's total energy supply, with solar and wind accounting for more than 70% of the total renewable generation share. A significant portion of this energy transition is taking place in households and buildings, which are incorporating local Photovoltaic (PV) generation to reduce electricity costs, and improve reliability when accompanied by storage, especially in jurisdictions with high solar radiation and regulators offering incentives [2]. Thus, some locations are experiencing a significant growth in small-scale PV installations, as in California, USA, which has 10.4 GW of such solar PV installations [2]. With such large-scale penetration of solar PV resources into the grid in the past few years, the California Independent System Operator (CAISO) started to notice that on certain days of the year, its net demand (demand net of renewable generation) dipped during the mid-afternoon, i.e., a "belly", that quickly ramped up to produce an "arch" (neck) in the evening. Such a demand curve came to be known as the "duck curve" [3]. Some challenges that arise for power system operators from such duck curve demand profiles are the oversupply of generation during the valley hours and short-steep ramps in the evening. Typically the solutions to this problem would seek to flatten the demand curve by appropriate use of Energy Storage Systems (ESSs), adding more flexible resources, and electrification of transportation, to name a few. This paper discusses the use of Demand Response (DR) as another tool to address this problem.

Some works have proposed the control of Heating, Ventilation and Air Conditioning (HVAC) systems to provide DR services to the grid. For example, [4] compares model-based and data-driven control approaches for DR applications based on HVACs systems. In the first approach a simple Resistance-Capacitance (RC) model is used to represent the thermal dynamics of houses, which are aggregated to reduce utility-level demand, while also minimizing their own electricity cost and discomfort level. In the second, the data-driven approach alleviates the need for house modeling and reduces computational times. However, the proposed controller requires modelling an Energy Management System (EMS) per household, which makes this approach impractical for load aggregation.

The authors of [5] propose an adaptive control strategy to turn ON and OFF the HVAC systems in residential buildings, considering external factors such as temperature and solar irradiance, as well as the household's internal heat gains. The proposed control dynamically adjusts its gains to compensate for imperfect information or disturbances in the household parameters. A second control layer tracks the power of the aggregated households and modifies the HVAC dispatch to minimize the error of the desired and actual system HVAC load profile. The proposed control law requires full knowledge of each household's thermal parameters, while its capability of handling different household temperature set-points is not demonstrated. A similar approach is discussed in [6], where a bi-level control strategy is proposed for residential aggregation of HVAC systems, with the upper and lower control layers minimizing a DR event-related electricity consumption and end-user discomfort level, respectively.

In [7], the operation of HVAC and a Battery Energy Storage

System (BESS) is optimized to provide DR in a building, using the thermal mass of the building to store thermal energy. The HVAC system is scheduled to minimize the total energy cost of the building, given higher prices at peak hours, while maintaining the comfort level within an acceptable range. A discrete-time Auto-regressive with exogenous input (ARX) model is used for the HVAC, whose parameters are obtained using parameter identification techniques and building simulation data. The authors show through simulations that the optimized HVAC schedule reduces the overall energy costs with respect to other alternatives, such as pre-cooling or constant temperature set points. However, these results are based on a building with a dedicated BESS, which adds storage capacity to the existing thermal mass of the house, but has a relatively large investment cost. Furthermore, the proposed thermal model requires significant tuning using reference data, and its application to load aggregation is not considered.

In [8], the temperature set-points of the HVAC systems are controlled to minimize the average discomfort level of the users, while satisfying a specified DR requirement. The proposed model includes the effects of humidity, solar radiation and wind speed on the indoor temperature perception of end users, and assumes a centralized approach, where all thermostat set-points are remotely controlled by a centralized entity, which could potentially discourage large-scale participation of users in such a DR program.

Reference [9] studies simple pre-cooling strategies to shift the A/C operation from peak to off-peak hours for households located in different cities in the USA, for various ambient conditions and two basic household structures. Such strategies comprise a single pre-cooling period with a thermostat set-point of 1° to 3 °C below the desired settings, before the utility peak-period, followed by another period of either the desired temperature setting or 1 °C above it; the former aims at maximizing energy savings, while the latter minimizes the coincident A/C peak demand. A large number of scenarios are considered, which comprise seven locations for 7-month simulation periods. The pre-cooling periods are designed to either maximize the energy savings or minimize the coincident peak demand. The results show energy savings between 1% to 8% for the maximum energy savings case, and up to 100% of demand savings for the coincident demand minimization case. We build on the approach in [9], addressing also the issue of aggregation.

Being a relatively new problem, few works have attempted to address the duck-curve issues by means of conventional strategies. For example, the work in [10] discusses an optimal unit commitment model to compensate for net load ramps by dispatching thermal units, Pumped Storage Hydro (PSH), fuel cells, and controllable loads in smart houses, also including DR via real time energy pricing. However, flattening the duck-curve is not addressed directly, but is rather a side effect of minimizing the fuel and start-up costs of the thermal units. A similar idea is developed in [11], but Compressed Air Energy Storage (CAES) is considered instead. The work in [12] proposes limiting the ramp rate of conventional generators during the neck portion of the duck-curve using Battery Energy Storage Systems (BESS); however, this approach required a

12.92 MWh BESS for a system load of 3.83 MW, making it economically infeasible. The authors in [13] propose a Model Predictive Control (MPC) based EMS that dispatches BESSs to provide the fast ramping requirement of the duck-curve, leading to a similar economically infeasible solution as [12], i.e., 130 MWh of BESS was necessary to provide the duck-curve ramping when 230 MW of PV was installed. Other studies based on ESSs include [14], where the storage capacity required to avoid solar curtailment in a duck-shaped load system is identified, which also recommends large ESS capacity to address this problem.

DR programs have also been proposed to address the duck-curve related issues. For example, [15] proposes a non-cooperative Stackelberg game and dynamic pricing to control the HVAC systems and BESS for end-users, to flatten the system demand curve. The methodology is based on a leader (system level grid operator) finding hourly energy prices for a given demand, which are sent to followers (end-users), who dispatch their local resources (BESS and HVAC), sending their load information back to the leader, who calculates new prices. This process is repeated until convergence is reached. The authors demonstrate that this approach can considerably flatten the system demand curve. In the work, each house is represented by simplified first-order thermal differential equations, assuming that their thermostat set-points are continuously and automatically defined by local controllers, which may not be practical.

The design of economic incentives for residential customers that could reduce the duck-curve ramp rates is studied in [16]. The authors assume that customers have BESSs and Heat Pump Water Heaters (HPWHs) as local controllable resources, whose operations are optimized by an EMS to reduce the customers' energy bills, considering uncertainty in the electrical load, hot water demand, and PV output. The designed incentive helps modify the dynamic selling and purchasing prices of energy, so that the combined operation of the household assets flattens the net demand curve. This methodology requires reliable bi-directional communication between aggregators and customers in order to be effective. Likewise, [17] discusses a DR program based on controllable loads of residential customers in the presence of a duck-curve demand profile. The program switches the appliances on and off depending on energy prices; however, the DR strategy is evaluated for a single house, and thus its effectiveness on the system duck-curve is not really assessed. Other works such as [18] and [19] propose the coordinated operation of Electric Vehicles (EVs) to reduce the load ramping requirements in systems with duck-curve profiles. However, the existing penetration levels of Electric Vehicles (EV)s and the current infrastructure and technology limitations to regulate EV charging rates are barriers that need to be overcome before considering this as a viable mitigation strategy.

From the aforementioned review, it is clear that ESSs and appropriate price signals are two of the most promising alternatives to deal with duck-curves; however, they also call for large investments in ESSs and a complex EMS infrastructure at the household level. In addition, most of the proposed HVAC control-based approaches require significant commu-

nication infrastructure, and require detailed information of the households being aggregated. A less infrastructure-dependent, simpler-to-implement, yet potentially effective measure that has not been studied in detail to flatten the duck-curve is the possible use of the thermal mass of households as an ESS. This strategy entails pre-cooling the households at times when PV generation is high, and to reduce or avoid the operation of air conditioner (A/C) loads during early evening hours. Hence, the main objective of this paper is to investigate the technical feasibility of longer duration pre-cooling, by performing detailed thermal simulations of households, and extending the results to the system level using an aggregated demand model based on probability distributions, which eliminates the need for detailed aggregated household modeling parameter data. Note that the market mechanisms such as incentives or prices to facilitate the adoption of the proposed approach are not fully evaluated in this paper; rather, the focus is on the technical aspects and their economic impact under the existing pricing mechanisms. However, note there may be other alternative uses for the local PV energy produced, such as EV charging or other energy storage approaches, that may be used to flatten the net house demand; these were not considered in this paper, since they are more complex and expensive techniques than the simple and practical pre-cooling methodology proposed here.

Commercial tools for detailed thermal simulation of buildings have been developed over the years and are widely available, such as EnergyPlus, Residential HVAC (RHVAC) or Air-Conditioning and Heating Engineers (APACHE). The main drawbacks of these tools are that they require extensive knowledge of thermal modelling with limited flexibility to adapt or add new models; cannot be readily integrated with other platforms to test EMS or DR strategies; and their core design was not meant to study interactions of electrical loads with thermal systems and local PV generation and storage. Hence, the Smart Residential Load Simulator (SRLS) developed at the University of Waterloo is used in this work for the time domain thermal simulations [20], with updates based on the more detailed household and solar irradiance models described in Section III-A. The SRLS is discussed and validated with actual home measurements in [20].

The rest of the paper is organized as follows: In Section II, the concept of the duck-curve and the main features of the SRLS are explained. In Section III, the proposed household thermal model, pre-cooling strategies and aggregated demand models are presented. In Section IV, the results of simulations to determine the feasibility of using pre-cooling in a household in three cities of USA, and the aggregated effects of different penetration levels of PV and adoption levels of pre-cooling on the system load demand in two US states are discussed. The main conclusions and future work are presented in Section V.

## II. BACKGROUND REVIEW

### A. The Duck-curve

The net demand of systems with abundant non-dispatchable PV generation connected at the distribution level is characterized by a duck curve [3], i.e., an U-shaped valley during the

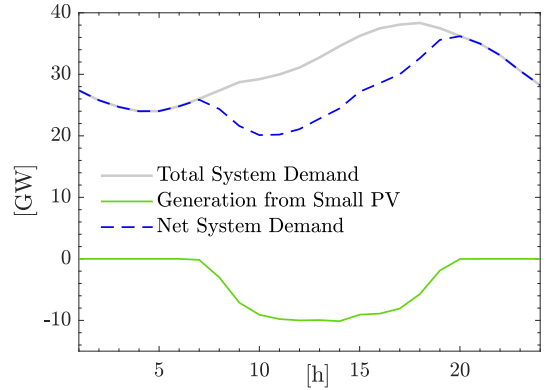


Fig. 1. Duck-curve California [22].

morning/day hours, ramping up as the evening approaches, as depicted in Fig. 1. The net load ramps up faster than the load ramp in the evening because of the reduction in solar production as the sun goes down. From an ISO's perspective, supplying such demand is challenging because it leads to over-supply of generation during the valley hours while requiring short-duration steep generation ramps to follow the demand when the solar resources dim down. Some strategies to mitigate these issues are [3]: increasing the net demand during the day by selling power to neighbouring markets; electrification of transportation, whereby more EVs could charge during the valley hours; introduce Time-of-Use (ToU) tariffs to shift the consumption to morning hours; make provisions for increased flexible resources in the power system so as to more quickly follow the ISO's instructions, possibly including curtailment of residential solar production [21]; increase ESS installations; and DR programs, which is the approach discussed here.

### B. Smart Residential Load Simulator

The SRLS is a freeware developed at the University of Waterloo, Canada, which allows thermal and electrical energy modeling of a household, to study the EMS in smart grids [20]. The SRLS comprises electrical, mechanical, and thermal models of typical appliances and HVAC systems available in modern homes and includes models for PV generation and BESSs. It allows simulating on/off decisions for some residential appliances, including stove, dryer, lighting, washing machine, pool pump, and dishwasher, by defining their schedules and basic parameters, such as efficiencies and ratings. On the other hand, water heater, HVAC and the refrigerator operates automatically, based on external variables and parameters such as ambient and house temperatures and occupancy. Additional software features, model details and validation can be found in [20]. The improved thermal model of the house and solar irradiance models discussed in the following sections, have been implemented for the studies presented here, and are available in the most recent version of the SRLS (V2.4) [23].

## III. MODELS

### A. Household Thermal Model

The temperature inside the house depends on the external weather conditions, particularly temperature and solar radia-

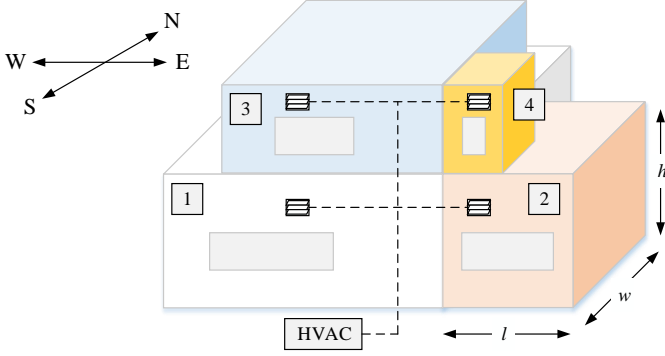


Fig. 2. Generic household topology.

tion and internal characteristics such as room size, construction material, type of windows, house orientation and location; and internal heat sources such as HVAC systems, air circulation through open areas and heat produced by people and appliances. The main assumptions of the house thermal model described in this sections are [24]:

- The outdoor temperature is the same for all the external walls of the house, including its roof.
- Heat is transferred through walls by conduction only.
- The solar radiation onto external walls accumulates in their thermal mass.
- The solar radiation passing through the windows accumulates in the house's internal thermal mass.

Outdoor temperature and solar irradiance data can be reliably obtained from meteorological stations, and is usually freely available (e.g., at [25]). Based on [24], the thermal characteristics of the household are represented here by the thermal capacitance  $C$  (thermal mass) and thermal resistance  $R$  of the house's internal and external walls, windows, and rooms' space and furniture, the values of which are functions of the geometry and material of these spaces. Internal walls are those shared by rooms, while external walls are those surrounding the house, including roof and floor. The area of the internal and external walls and windows of a generic house, such as the one depicted in Fig. 2, can be defined by a set of matrices and vectors, as follows:

$$E_{i,m} = -W_{i,m} + \begin{cases} l_i h_i & \text{if } m = \{1, 2\} \\ w_i h_i & \text{if } m = \{3, 4\} \\ l_i w_i & \text{if } m = \{5, 6\} \end{cases} \quad (1)$$

$$B_{i,j} = \sum_m^6 E_{i,m} V_{i,j,m} \quad (2)$$

$$O_{i,m} = E_{i,m} - E_{i,m} \sum_j^n V_{i,j,m} \quad (3)$$

where  $i$  and  $j$  are room indices;  $m$  is a wall orientation index which can have values from 1 to 6, corresponding to walls facing north, south, east, west, up and down, respectively; and  $W_{i,m}$  is the equivalent area of room  $i$  window located on the wall in direction  $m$ . The entries of vectors  $\mathbf{l} \in \mathbb{R}^n$ ,  $\mathbf{h} \in \mathbb{R}^n$ ,  $\mathbf{w} \in \mathbb{R}^n$  contain the length, height and width of room  $i$  for  $n$  rooms;  $\mathbf{E} \in \mathbb{R}^{n \times 6}$  contains the wall areas of each room

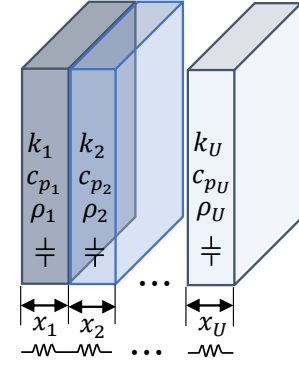


Fig. 3. Multi-layer wall/window model.

$i$  in all directions  $m$ ;  $V_{i,j,m}$  are entries of a sparse topology matrix  $\mathbf{V} \in \mathbb{R}^{n \times n \times 6}$ , representing the fraction of  $E_{i,m}$  that is common to room  $j$ , in the direction  $m$ , while the condition  $\sum_j^n V_{i,j,m} \leq 1$ , which must be satisfied, limits to 1, the total fraction of wall area shared with other rooms;  $\mathbf{B} \in \mathbb{R}^{n \times n}$  and  $\mathbf{O} \in \mathbb{R}^{n \times 6}$  contain the internal and external rooms' wall areas. Thus, the wall matrix  $\mathbf{A} \in \mathbb{R}^{n \times n}$  can be defined using diagonal entries  $A_{ii}$  denoting the total external wall area of room  $i$ , and off-diagonal elements  $A_{ij}$  the internal wall areas between rooms  $i$  and  $j$ , as follows:

$$A_{i,j} = \begin{cases} \sum_m^6 O_{i,m} & \text{if } i = j \\ B_{i,j} & \text{if } i \neq j \end{cases} \quad (4)$$

From (4), the thermal parameters of the house can be calculated as follows [26]:

$$R_{w_{ij}} = \frac{1}{A_{i,j}} \sum_u^U \frac{x_u}{\mathcal{K}_u}, \quad R_{f_i} = \frac{1}{O_{i,6}} \sum_u^U \frac{x_u}{\mathcal{K}_u} \quad (5)$$

$$C_{w_{ij}} = A_{i,j} \sum_u^U c_{p_u} \rho_u x_u, \quad C_{f_i} = O_{i,6} \sum_u^U c_{p_u} \rho_u x_u \quad (6)$$

$$R_{c_i} = \frac{1}{\sum_m^6 W_{i,m}} \sum_u^U \frac{x_u}{\mathcal{K}_u} \quad (7)$$

where  $R_{w_{ij}}$  and  $C_{w_{ij}}$  are the total equivalent thermal resistance and thermal capacitance, respectively, of the internal walls  $ij$  ( $i \neq j$ ) between rooms or external walls of room  $i$  ( $i = j$ ), which comprise  $U$  layers of thickness  $x_u$ , thermal conductivity  $\mathcal{K}_u$ , density  $\rho_u$ , and specific heat capacity  $c_{p_u}$ , as depicted in Fig. 3;  $R_{c_i}$  is the thermal resistance of the window in room  $i$ ; and  $R_{f_i}$  and  $C_{f_i}$  are the thermal resistance and capacitance of room's  $i$  floor, respectively, modeled only for those rooms having contact with the ground. Note that the thermal mass of windows is not modeled, but rather represented by its thermal resistance only [27]. The thermal mass of each room comprises the air occupying its volume and any furniture in the room; hence, the room's thermal capacity can be calculated as follows [20]:

$$C_{in_i} = l_i w_i h_i [(1 - \Omega) \rho_{air} c_{p_{air}} + \Omega \rho_{wood} c_{p_{wood}}] \quad (8)$$

where  $\rho_{air}$  and  $\rho_{wood}$  are densities of air and wood, respectively;  $c_{p_{air}}$  and  $c_{p_{wood}}$  are the specific heat capacities of air

and wood, respectively; and  $\Omega$  is the fraction of room volume occupied by furniture.

By balancing the thermal energy in a room, the following differential equations can be obtained [20]:

$$C_{w_{ii}} \dot{T}_{w_{ii}} = \frac{T_{am} + T_{in_i} - 2T_{w_{ii}}}{R_{w_{ii}}/2} + Q_{sr_i} \quad (9)$$

$$C_{f_i} \dot{T}_{f_i} = \frac{T_g + T_{in_i} - 2T_{f_i}}{R_{f_i}/2} \quad (10)$$

$$C_{w_{ii}} \dot{T}_{in_i} = \sum_j^n \frac{T_{w_{ij}} - T_{in_i}}{R_{w_{ij}}/2} + \frac{T_{am} - T_{in_i}}{R_{c_i}} \quad (11)$$

$$+ \mu_i (Q_{in} + Q_{HVAC}) + Q_{c_i} + \frac{T_{f_i} - T_{in_i}}{R_{f_i}/2}$$

where  $T_{am}$  and  $T_g$  are the ambient and ground temperatures, respectively;  $Q_{sr_i}$  is the solar radiation heating power affecting the external walls;  $Q_{c_i}$  is the solar radiation on the windows;  $Q_{in}$  represent the heat produced by active people in the house;  $Q_{HVAC}$  is the heating power of the central HVAC system, which takes negative values if it works in cooling mode (e.g., A/C), and positive in heating mode (e.g., furnace); and  $\mu_i$  is a factor that distributes  $Q_{HVAC}$  among the rooms, as depicted in Fig. 2, such that  $\sum_i \mu_i = 1$ . An equivalent thermal circuit for (9) and (11) is depicted in Fig. 4. Note that (10) and the last term of (11) are only considered when modeling rooms whose floors are in contact with the ground. Note that the model assumes that the heat from solar radiation passing through windows and falling onto external walls is stored in the room's internal thermal mass and external walls' thermal mass, respectively, and can be approximated as follows [28]:

$$Q_{c_i} = SHGC \sum_m^5 W_{i,m} I_m \quad (12)$$

$$Q_{sr_i} = \kappa\tau \sum_m^5 O_{i,m} I_m \quad (13)$$

where  $SHGC$  is the Solar Heat Gain Coefficient, which is the fraction of solar radiation admitted through the windows and released inside the house;  $\tau$  and  $\kappa$  are the transmittance and absorptance of the external walls, which represent the fraction of solar radiation passing the external wall layer, and absorbed in the insulation layer, respectively; and  $I_m$  is the solar irradiance incident on the external wall facing the direction  $m = \{1, \dots, 5\}$ , calculated as follows [29]–[31]:

$$I_m = I_b \cos \theta_m + (I_b \sin \zeta + I_h) \vartheta \left( \frac{1 - \cos \psi_m}{2} \right) \quad (14)$$

$$+ I_h \left[ (1 - F_1) \left( \frac{1 + \cos \psi_m}{2} \right) + F_1 \left( \frac{a}{b} \right) + F_2 \sin \psi_m \right]$$

$$\cos \theta_m = \sin \delta (\sin \phi \cos \psi_m + \cos \phi \sin \psi_m \cos \gamma_m) \quad (15)$$

$$+ \cos \delta \cos \omega (\cos \phi \cos \psi_m - \sin \phi \sin \psi_m \cos \gamma_m)$$

$$- \cos \delta \sin \psi_m \sin \gamma_m \sin \omega$$

$$\sin \zeta = \sin \phi \sin \delta + \cos \phi \cos \delta \cos \omega \quad (16)$$

$$\delta = 23.45^\circ \sin \left( 360 \frac{284 + day}{365} \right) \quad (17)$$

$$\omega = 15t_H - 180^\circ \quad (18)$$

$$F_1 = F_{11} + F_{12}\Delta + F_{13}z \quad (19)$$

$$F_2 = F_{21} + F_{22}\Delta + F_{23}z \quad (20)$$

$$\psi_m = \begin{cases} 90^\circ & \text{if } m = 1, 2, 3, 4 \\ 0^\circ & \text{if } m = 5 \end{cases} \quad (21)$$

$$\gamma_m = \begin{cases} 0^\circ & \text{if } m = 1, 5 \\ 180^\circ & \text{if } m = 2 \\ 90^\circ & \text{if } m = 3 \\ 270^\circ & \text{if } m = 4 \end{cases} \quad (22)$$

$$\mathcal{B} = \left( \frac{I_h}{1361} \right) \frac{1}{\sin \zeta}; \quad z = (90^\circ - \zeta) \frac{\pi}{180^\circ} \quad (23)$$

$$a = \max(0, \cos \theta_m); \quad b = \max(\cos(85^\circ), \sin \zeta) \quad (24)$$

where  $I_m$  is the total solar irradiance normal to the surface;  $I_b$ ,  $I_h$ , and  $(I_b \sin \zeta + I_h)$  are the beam, horizontal diffuse, and global horizontal solar irradiance, respectively;  $\theta_m$  is the incidence angle to the external walls in the direction  $m$ ;  $\zeta$  is the solar altitude angle;  $\psi_m$  and  $\gamma_m$  are the inclination angle and azimuth angle (measured clock-wise from the north) of walls facing the direction  $m$ ;  $\omega$  is the hour angle;  $t_H$  is the day time in hours;  $\phi$  is the latitude;  $F_1$  and  $F_2$  are coefficients that describe circumsolar and horizon brightness, respectively;  $\vartheta$  is the hemispherical ground reflectance;  $\mathcal{B}$  is the sky brightness parameter; and  $a$ ,  $b$ , and  $z$  are auxiliary variables. The coefficients  $F_{11}$ ,  $F_{12}$ ,  $F_{13}$ ,  $F_{21}$ ,  $F_{22}$ ,  $F_{23}$  can be obtained from [29].

The internal heat gains can be calculated as follows:

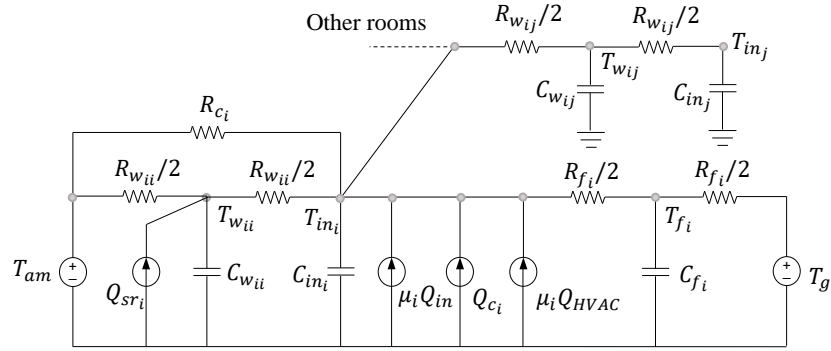
$$Q_{in} = \xi_t Q_{pl} \quad (25)$$

where  $\xi_t$  is the number of active people in the house at time  $t$ , and  $Q_{pl}$  is the heating power generated by each active individual in the house.

Note that the proposed house thermal model assumes the same construction materials for all walls and windows, which affects its accuracy when more complex house structures need to be modeled. Furthermore, since rooms are not connected through open space (only through walls), air circulation and the effects of shades cast onto the walls are not considered either.

*1) Household Pre-cooling Strategies:* In summer most households set their thermostats at lower temperatures when home and higher when away, e.g., 22°C and 25°C, respectively [32]. Hence, assuming that people leave the house at 09:00 and return at 18:00, 22°C and 25°C are used as set points here, which will be referred to as Business as Usual (BAU) without pre-cooling strategy, as shown in Fig.5.

The objective of pre-cooling is to reduce the house temperature in advance, before the evening reduction in solar production, so that the A/C operates at a lower duty cycle during these evening hours. Hence, simple pre-cooling strategies are considered here, based on [9], given that such an approach is more likely to be adopted due to its simpler implementation in practice. Such strategies comprise a single pre-cooling period

Fig. 4. Thermal circuit of room  $i$ .

with a thermostat set point of 1 to 3°C below the desired settings, before the utility peak-period, followed by another period of either the desired temperature setting, or 1°C above it before returning to the desired temperature setting, to reduce the A/C usage at peak demand hours, given the higher prices of electricity at these hours. Hence, the length and starting time of the pre-cooling period are the main tunable parameters, which can be determined through thermal simulations, presented in the next section.

The required pre-cooling period depends on the ambient conditions and household thermal characteristics. In this paper, the pre-cooling strategies aim to improve the house net demand load factor, thus helping to reduce the system duck-curve when multiple houses are aggregated. The end of the pre-cooling period is selected so that the temperature in the house around the peak-hours remains within a specified comfort level, without the help of the A/C. On the other hand, the beginning of the pre-cooling period is varied to maximize the PV energy use by the A/C. Hence, the following three simple pre-cooling strategies with increasing pre-cooling periods, illustrated in Fig. 5, are considered:

- 1) *3h Pre-cooling*: The thermostat is set to 19°C, which is three degrees below the desired temperature (22°C) for three hours before residents arrive home, and at a higher temperature of 23°C, which is 1 degree above the desired temperature for another three hours after arriving home.
- 2) *4h Pre-cooling*: The house is pre-cooled at 19°C, from 13:00 to 17:00, followed by a period of a higher set-point (23°C), and then returning to the target temperature of 22°C at 21:00. Note that in this strategy, the pre-cooling period starts earlier and lasts longer, to increase the PV energy utilization.
- 3) *7h Pre-cooling*: The house is pre-cooled at 19°C, from 10:00 to 17:00, followed by a period of a higher set-point (23°C), and then returning to the target temperature of 22°C at 21:00.

### B. Aggregated Demand Model

The proposed methodology for modeling the aggregated demand uses the load profile of a benchmark household to randomly generate new profiles based on probability distributions, so that their aggregation resembles a reference system demand

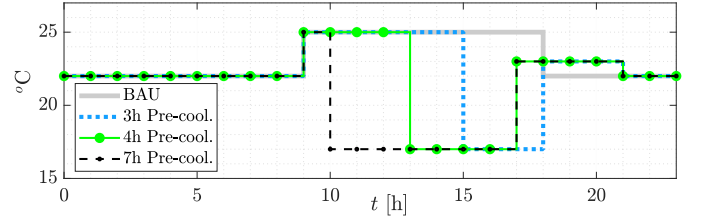


Fig. 5. Proposed BAU and pre-cooling strategies for A/C thermostat setpoints.

profile, e.g., California or Texas, USA. It assumes that the A/C in the benchmark household follows the BAU cooling strategy. An optimization problem is solved to minimize the error of the model's demand prediction by adjusting its parameters, which are the standard deviations of the distributions. Finally, when the model is trained, a series of random simulations are used to generate household load profiles combining the BAU and one of the pre-cooling strategies, which allows simulating different adoption levels of pre-cooling. The methodology is summarized in Fig. 6, and each step of the process, identified by a number on the left corner of the corresponding box, is explained next.

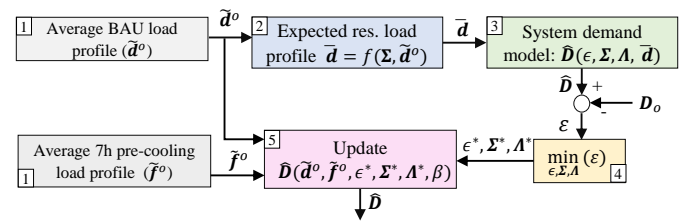


Fig. 6. Proposed aggregated demand methodology.

*Step 1*: The data resolution of the detailed benchmark house load profiles obtained from time domain simulations, based on the thermal models introduced in Section III-A, is much higher than the resolution of typical hourly system demand profiles available; therefore, averaging of the former over time is necessary, as depicted in Fig. 7. Hence, the average house load profile for the BAU strategy  $\tilde{\mathbf{d}}^o = [\tilde{d}_1^o, \dots, \tilde{d}_N^o]^T$ , pre-cooling  $\tilde{\mathbf{f}}^o = [\tilde{f}_1^o, \dots, \tilde{f}_N^o]^T$ , and the household PV generation

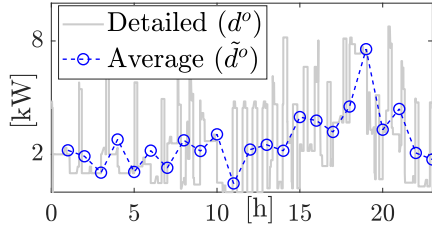
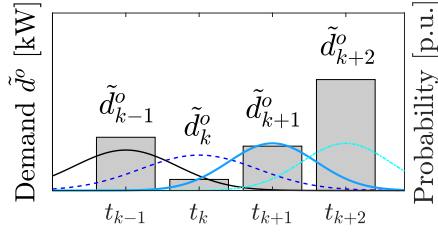


Fig. 7. Benchmark house load profile.

Fig. 8. Normal probability distribution centered at time  $t_i$ .

$\tilde{g}^o = [\tilde{g}_1^o, \dots, \tilde{g}_N^o]^T$  can be calculated, as follows:

$$\tilde{d}_k^o = \frac{\sum d_h^o}{M}, \quad \tilde{f}_k^o = \frac{\sum f_h^o}{M}, \quad \tilde{g}_k^o = \frac{\sum g_h^o}{M} \quad (26)$$

where  $k$  is the index of the  $N$  data points of the average load profiles;  $\mathbf{t} = [t_1, \dots, t_N]^T$  is a time vector associated with the average load profiles, and thus  $\Delta t = t_{k+1} - t_k$  is the time resolution of the average load profile data;  $d_h^o$  are data points of the high-resolution detailed house load profiles for BAU;  $h$  is the index of data points in the high-resolution load profile vectors  $\mathbf{d}^o$ ; and  $M$  is the number of data points in the interval  $[t_k, t_{k+1}]$ . In this paper, the data resolution is expressed in terms of  $\Delta t$ , e.g.,  $\Delta t=1\text{h}$ ,  $\Delta t=0.5\text{h}$ , etc.

*Step 2:* The estimated average electrical load in the BAU strategy,  $\hat{d}_k^s$  at time  $t_k$  of another household  $s$ , may not necessarily be the same as  $\tilde{d}_k^o$  of the benchmark household. Indeed,  $\hat{d}_k^s$  has two dimensions of differences, size and time, where size refers to the magnitude of  $\hat{d}_k^s$ , which is associated with the ratings of the appliances, and time referring to the effective time  $t_k$  when this demand takes place in household  $s$ , the value of which is influenced by its inhabitants' behaviour. For example, the washing machine of one customer could be turned on at 10:00, while at 11:00 by another. In general, typical appliances as those considered here tend to operate in relatively narrow windows of, for example, two hours, across all households. The time dimension of  $\hat{d}_k^s$  could be described as a normally distributed random process, as per the central limit theorem. Hence, by defining  $N$  normally distributed random variables  $\mathcal{T}_k \sim \mathcal{N}(t_k, \sigma_k^2)$  to represent the time at which the demand  $\hat{d}_k^o$  effectively occurs in any household (Fig. 8), where the mean is  $t_k$  for a standard deviation  $\sigma_k$ , the following probability square matrix can be defined:

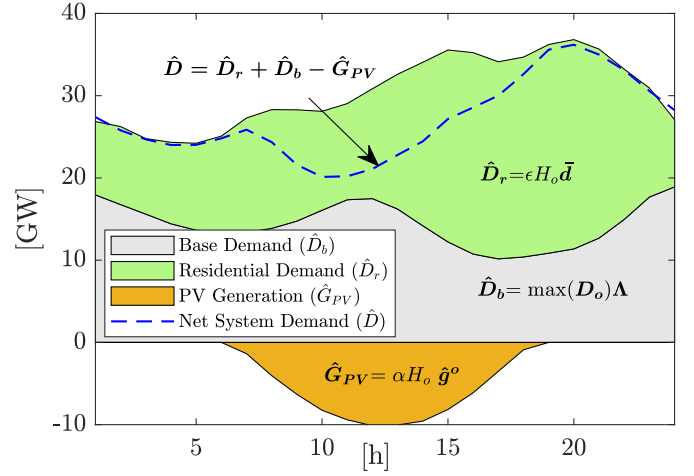


Fig. 9. Estimated system demand components.

$$\mathbf{P} = \begin{bmatrix} P_{1,1} & \dots & P_{1,k} & \dots & P_{1,N} \\ \vdots & & \vdots & & \vdots \\ P_{k,1} & \dots & P_{k,k} & \dots & P_{k,N} \\ \vdots & & \vdots & & \vdots \\ P_{N,1} & \dots & P_{N,k} & \dots & P_{N,N} \end{bmatrix} \quad (27)$$

where, for example,  $P_{k,1} = p(\mathcal{T}_k = t_1)$  corresponds to the probability of demand  $\hat{d}_k^o$  occurring at time  $t_1$ .

*Step 3:* From (27), the expected value of any house's demand at time  $t_k$  can be calculated as follows:

$$\bar{d}_k = P_{1,k}\tilde{d}_1^o + \dots + P_{k,k}\tilde{d}_k^o + \dots + P_{N,k}\tilde{d}_N^o, \quad \forall k = 1, \dots, N \quad (28)$$

where  $P_{k,k}$  are entries of the probability matrix  $\mathbf{P}$ . Hence, the expected load profile vector  $\bar{\mathbf{d}}$  can be calculated as follows:

$$\bar{\mathbf{d}}(\boldsymbol{\Sigma}, \tilde{\mathbf{d}}^o) = \mathbf{P}^T \tilde{\mathbf{d}}^o \quad (29)$$

where  $\boldsymbol{\Sigma} = [\sigma_1, \dots, \sigma_k, \dots, \sigma_N]^T$ .

*Step 4:* The proposed net aggregated system demand model contains three components: residential demand  $\hat{D}_r$ ; base demand  $\hat{D}_b$ , which includes other types of demand, such as commercial, industrial, public lighting, EVs, etc.; and PV generation  $\hat{G}_{PV}$ , representing photovoltaic generation embedded in the distribution systems, and thus, not directly observed by the ISO. Hence, the proposed net aggregated system demand  $\hat{D}$  can be calculated as follows:

$$\hat{D} = \hat{D}_r + \hat{D}_b - \hat{G}_{PV} \quad (30)$$

$$\hat{D}_r = \epsilon H_o \bar{\mathbf{d}}(\boldsymbol{\Sigma}, \tilde{\mathbf{d}}^o) \quad (31)$$

$$\hat{D}_b = \max(\mathbf{D}_o) \boldsymbol{\Lambda} \quad (32)$$

$$\hat{G}_{PV} = \alpha H_o \tilde{g}^o \quad (33)$$

where  $H_o$  is the total number of existing households in the system, while  $\epsilon$  is the fraction of those households with expected demand  $\bar{\mathbf{d}}$ ;  $\mathbf{D}_o = [D_{o_1}, \dots, D_{o_k}, \dots, D_{o_N}]^T$  is the reference system demand vector;  $\boldsymbol{\Lambda} = [\lambda_1, \dots, \lambda_k, \dots, \lambda_N]^T$  is a vector whose entries  $\lambda_k$  represent the fraction of  $D_{o_k}$  that

corresponds to the base load; and  $\alpha$  is the fraction of houses  $H_o$  with PV systems of an equivalent generation profile  $\tilde{g}^o$ . Note that this model assumes a simple aggregation for  $\hat{G}_{PV}$  assuming, for simplicity, that all distributed PV injections in the households are highly correlated in time; hence, the parameter  $\alpha$  can be defined as follows:

$$\alpha = \frac{\max(PV_{sys})}{H_o \max(\tilde{g}^o)} \quad (34)$$

where  $PV_{sys}$  is the total PV generation by residential systems connected at the distribution system level.

In order to find the model parameters  $(\epsilon, \Sigma, \Lambda)$ , the following optimization problem is solved:

$$\min_{\epsilon, \Sigma, \Lambda} J_{err} + \Psi J_{var} \quad (35)$$

$$\text{s.t. } J_{err} = \frac{1}{N} \left\| \frac{(\hat{D}_r + \hat{D}_b - \hat{G}_{PV}) - D_o}{\max(D_o)} \right\|_2 \quad (36)$$

$$J_{var} = \sum_k^{N-1} (\lambda_{k+1} - \lambda_k)^2 \quad (37)$$

$$\max(D_o) \Delta t \sum_k^N \lambda_k \leq \chi \sum_k^N D_{o_k} \Delta t \quad (38)$$

$$0 \leq \epsilon \leq 1 \quad (39)$$

$$\mathbf{0} \preceq \Lambda \preceq \mathbf{1} \quad (40)$$

$$\mathbf{0} \preceq \Sigma \preceq \sigma_{\max} \mathbf{1} \quad (41)$$

where the multi-objective function (35) seeks to minimize the Mean Squared Error (MSE) of the model prediction (36), while keeping the base demand curve (37) smooth, based on the regularization parameter  $\Psi$ . Constraint (38) ensures that at least  $\chi$  fraction of the total daily system energy corresponds to residential demand, and constraints (39) to (41) define limits for the problem variables  $\epsilon$ ,  $\Sigma$ , and  $\Lambda$ .

*Step 5:* With the optimal model parameters  $\epsilon^*$ ,  $\Sigma^*$ , and  $\Lambda^*$ , simulations are used to aggregate  $S$  number of BAU-based house random load profiles  $\hat{d}^s$ , and  $L$  number of pre-cooling house random load profiles  $\hat{f}^l$ , such that  $S + L = \epsilon H_o$ ; hence (30) can be written as follows:

$$\hat{D} = \left[ \sum_s^S \hat{d}^s + \sum_l^L \hat{f}^l \right] + \max(D_o) \Lambda^* - \alpha H_o \tilde{g}^o \quad (42)$$

$$S = (1 - \beta) \epsilon^* H_o \quad (43)$$

$$L = \beta \epsilon^* H_o \quad (44)$$

where  $\beta \in [0, 1]$  is a factor that defines the adoption level of pre-cooling in the system, corresponding to households with pre-cooling potential. For example,  $\beta=0.25$  means that 25% of  $\epsilon H_o$  houses apply the pre-cooling strategy, while 75% of them use a BAU strategy; this assumes that at least 25% of the houses in the system are capable of applying pre-cooling, and thus have the required thermal characteristics, with the remaining 75% profiles of the households that do not participate in this DR program being generated from the BAU reference profile assuming different thermal masses, wall insulation levels, A/C and appliances ratings, thermostat set

points, human activity levels, etc. The vectors  $\hat{d}^s$  and  $\hat{f}^l$  for each  $s$  and  $l$  can be calculated as follows:

$$\hat{d}^s = \mathbf{Z}_{pc}^T \tilde{d}^o, \quad \forall pc = 1, \dots, S \quad (45)$$

$$\hat{f}^l = \mathbf{Z}_{pc}^T \tilde{f}^o, \quad \forall pc = S + 1, \dots, S + L \quad (46)$$

where the  $\mathbf{Z}_{pc} \in \mathbb{R}^{N \times N}$  is a sparse matrix generated for each household  $pc$ , and has similar interpretation as the matrix  $\mathbf{P}$  in (27), i.e.,  $Z_{pc_k, q} = 1$  if the demand  $\tilde{d}_k^o$  occurs at time  $t_q$ , while the rest of the entries of the row  $k$  are equal to zero.

Note that the simple aggregation of PVs in (33) may not be accurate for systems covering a wide area, as the solar irradiance can considerably vary from one region to another. Furthermore, although the solution of the optimization problem in (35)-(41) guarantees an accurate estimated aggregated net system demand, the reference load profiles  $d^o$  and  $f^o$  should reflect a typical behaviour of a house within the system, and be modeled for similar ambient conditions. Finally, the proposed model can be used to aggregate the demand of any system size; however, it assumes that the majority of the households are typical two-story buildings, which may not be applicable for high-densely populated areas based on residential buildings.

#### IV. RESULTS AND COMPARISONS

The effectiveness of the BAU and three proposed pre-cooling strategies discussed in Section III-A1 is first evaluated through thermal simulations of a typical North American household, using the latest version of SRLS (V2.4) [23]. The household configuration, weather data, and ToU tariffs are discussed for three US locations, namely, Los Angeles in California, Austin in Texas, and Phoenix in Arizona, given their potential for large deployment of small-scale residential PV installations, which may result in duck-curve loading issues; in fact, California has already been experiencing these problems.

The aggregated system demand for California and Texas are then developed, based on the house load profiles obtained for Los Angeles and Austin, respectively, for different PV penetration levels and pre-cooling adoption scenarios, following the methodology described in Section III-B. For validation purposes, the measured aggregated net demand of 83 houses in a neighbourhood of Austin is compared with the aggregation of the same number of houses based on the proposed methodology for Texas. For lack of adequate data, Arizona was not considered for the aggregation case study. Finally, a statistical analysis of the aggregated demand is presented, and the system load factor is calculated to demonstrate the effectiveness of the proposed 7h pre-cooling to flatten the system's demand curve.

##### A. Household Thermal Simulations and A/C Load Profile

1) *Household Configuration:* The household model and its electrical demand is considered the same for the three locations studied. A typical North American house with a total surface area of 185 m<sup>2</sup> distributed in four room blocks was assumed, as depicted in Fig. 2. A 48,000 BTU/h (14.07 kW) central A/C unit with enough cooling power for the household

TABLE I  
ASSUMED HOUSE AND ROOM DIMENSIONS IN USA.

Parameter	Room 1	Room 2	Room 3	Room 4
$l_i$ (m)	8	4	8	4
$w_i$ (m)	9	9	9	4
$h_i$ (m)	2.7	2.7	2.7	2.7
$W_{i,2}$ (m <sup>2</sup> )	9.9	6	16.5	4.5

TABLE II  
SOLAR ENERGY RADIATION ONTO EXTERNAL WALLS AND A/C ENERGY CONSUMPTION FOR A DAY OF SIMULATION.

Location	Strategy	A/C Energy (kWh)			Irradiance (kWh/m <sup>2</sup> )		
		Window orientation			Wall orientation		
		South	East	West	South	East	West
L.A.	BAU	22.9	22.5	22.3	3.99	3.90	3.72
	7h P.	29.3	29.1	28.4			
Austin	BAU	29.7	27.3	27.7	3.30	2.77	3.10
	7h P.	35.4	32.9	33.9			
Phoenix	BAU	30.5	28.1	29.4	3.45	2.84	3.40
	7h P.	36.0	33.9	35.3			

was considered. The sizes of the rooms and windows are summarized in Table I. Note that all windows are assumed to be pointing south ( $m = 2$ ), which favours natural lighting and allows more solar radiation into the house; this assumption of orientation is the worst case scenario for cooling, as seen in Table II, which compares the total daily solar energy radiation per square meter onto the south, east and west walls for the three locations considered, as well as the A/C energy consumed in the BAU and 7h pre-cooling A/C operation strategies, assuming the household's windows are located in walls facing the three orientations. Observe that the south wall receives the highest solar radiation energy for the simulated day. Furthermore, the case of windows located in the south-facing walls results in the largest A/C energy consumption for all locations and A/C operation strategies simulated. These values were obtained based on (14)-(24), the beam and horizontal diffuse solar irradiance data and time domain thermal simulations. The thermal characteristics of walls and windows are summarized in Table III. The transmittance of a painted stucco surface (first layer of the external walls) is  $\tau = 0.35$  [33], while the absorptance of glass wool is  $\kappa = 0.24$  [34]. The windows are double-glazed with an intermediate layer of air, and an equivalent  $SHGC = 0.25$  as recommended in [35] for houses in southern regions of USA. Finally, based on estimations on a real house, it is assumed that 1.5% of a room volume is occupied by wooden furniture; thus,  $\Omega = 0.015$  in (8). The assumed household characteristics are consistent with existing building codes at the locations considered in the paper [36]–[38]; however, older residential building stock may have different characteristics that make them less suitable for pre-cooling.

The household has the following appliances and electric equipment [20]: fridge, dryer, stove, dish washer, washing machine, pool pump, A/C, and lighting. The power consumption profile of each appliance and the total household demand profile, excluding the A/C, whose consumption level depends on outdoor weather conditions, is presented in Fig.

TABLE III  
HOUSE THERMAL PARAMETERS.

Element	Layer	Material	$x$ cm	$k$ W/m.K	$\rho$ kg/m <sup>3</sup>	$c_p$ J/kg.K
External wall	1	Stucco	2	0.8	2,275	900
	2	Plywood	1	0.13	650	1,298
	3	Glass wool	9	0.038	220	795
	4	Drywall	1	0.5	724	852
Internal wall	1	Drywall	1	0.5	724	852
	2	Air	9	0.024	1,225	1005.4
	3	Drywall	1	0.5	724	852
Windows	1	Glass	0.4	0.81	-	-
	2	Air	0.8	0.024	-	-
	3	Glass	0.4	0.81	-	-

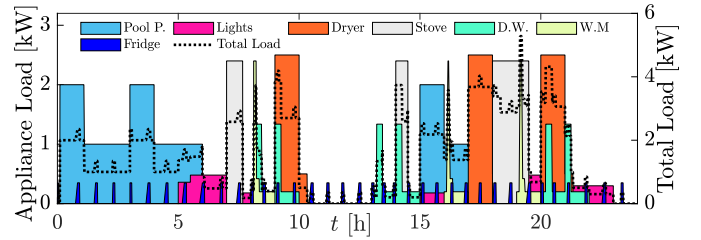


Fig. 10. Household demand profile excluding the A/C load.

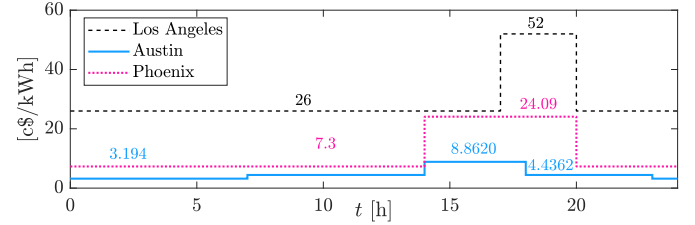


Fig. 11. Residential ToU tariffs in various US cities.

10. The scheduled operation of the appliances follow a typical behaviour of residential households for a weekday. The activity level  $\xi_t$  in (25) for five inhabitants was determined based on the methodology proposed in [39], where each active person contributes 92 W of heating power.

2) *Ambient Conditions and ToU Tariffs*: The household was assumed to be equipped with an 8 kW PV unit, with its power generated depending on the house location. The temperature, beam irradiance, horizontal diffuse irradiance and local PV generation were obtained from [25], for August 28, 2020 for Los Angeles and Phoenix, and August 26, 2020 for Austin, which were summer days with relatively high temperatures and uniform solar irradiance. The ToU tariffs for Los Angeles [40], Austin<sup>1</sup> [41] and Phoenix [42] are presented in Fig. 11 as obtained from local utilities. It is assumed here that PV injections to the grid are paid at the same price as the energy consumed, as per a net metering policy.

3) *Household Temperature and A/C Load Simulations*: The temperature of Room 1 for the three locations and pre-cooling strategies is presented in Fig. 12. Observe that, the thermal

<sup>1</sup>ToU rates from Pedernales Electric Coop, which is a utility serving areas outside of Austin, were used as a proxy to hypothetical ToU rates for Austin, since its local utility, Austin Energy, had pilot ToU rates in the past that are no longer available

mass of the house is large enough to allow the temperature to remain within  $17^{\circ}\text{C}$  and  $23^{\circ}\text{C}$ , from 18:00 to 21:00 in the 3h pre-cooling case, and 17:00 to 20:30 (21:00 in Austin) in the 4h and 7h pre-cooling cases, without using the A/C. On the other hand, Fig. 13 shows the moving average of the net demand for the same study cases. The negative values are due to the PV generation exceeding the house demand and is particularly prevalent during the middle of the day under BAU. The differences in the load profiles between the pre-cooling strategies are the result of changes in the A/C load only. Note that the 3h pre-cooling shifts the A/C load to afternoon hours, between 15:00 and 16:00, whereas when longer pre-cooling is adopted, the A/C operation is more uniformly distributed, particularly during morning hours. These results suggest that longer pre-cooling can reduce the PV injections to the grid as compared to the BAU and 3h pre-cooling cases, and could flatten the system duck-curve effect, while keeping the house temperature within acceptable comfort levels when the A/C is off.

Note that the pre-cooling strategies not only shift the A/C operation from peak hours, but also increase the household's energy consumption due to longer hours of A/C operation, particularly when the A/C brings the house temperature down to the pre-cooling thermostat setting of  $17^{\circ}\text{C}$ , i.e., between 10:00 and 13:00, and 13:00 to 16:00 for the 4h and 7h pre-cooling strategies, respectively. These results are summarized in Fig. 14, along with the cost of energy for each study case. Observe that under existing ToU tariff rates, the 3h and 4h pre-cooling reduce the energy bill of customers in Los Angeles, while the 7h one is more expensive. On the other hand, longer pre-cooling in Phoenix results in lower energy bills. Finally, the customer's energy bill in Austin increases for any pre-cooling strategy, because the price difference between the on- and off-peak hours in Austin is not significant, and the on-peak price starts early at 14:00.

The effectiveness of the proposed pre-cooling strategies to reduce the A/C cycling during peak hours is constrained by the household's thermal properties. For example, a sensitivity analysis of a household's thermal mass in Austin for Room 1's temperature and 7h pre-cooling is illustrated in Fig. 15. Observe that as the thermal mass decreases from 100% of its original value to 70%, the room's temperature reaches the thermostat set point faster in the evening, thus activating the A/C earlier. Indeed, a reduction of 30% would be sufficient to add about one and a half hours of A/C operation at peak hours, compared to the 100% thermal mass case. These effects, along with other parameter variations associated with different thermostat set points, wall thermal conductivity, A/C ratings, etc., on the household load profile, are accounted for in the aggregation process, discussed in the next section.

### B. Aggregated System Load Simulations

The model proposed in Section III-B is used to develop an aggregated demand model for a warm summer day in California (August 28, 2020) and Texas (August 26, 2020), based on the households' appliance load profiles (similar to those in Fig.10) and the A/C load profiles obtained in Section IV-A3

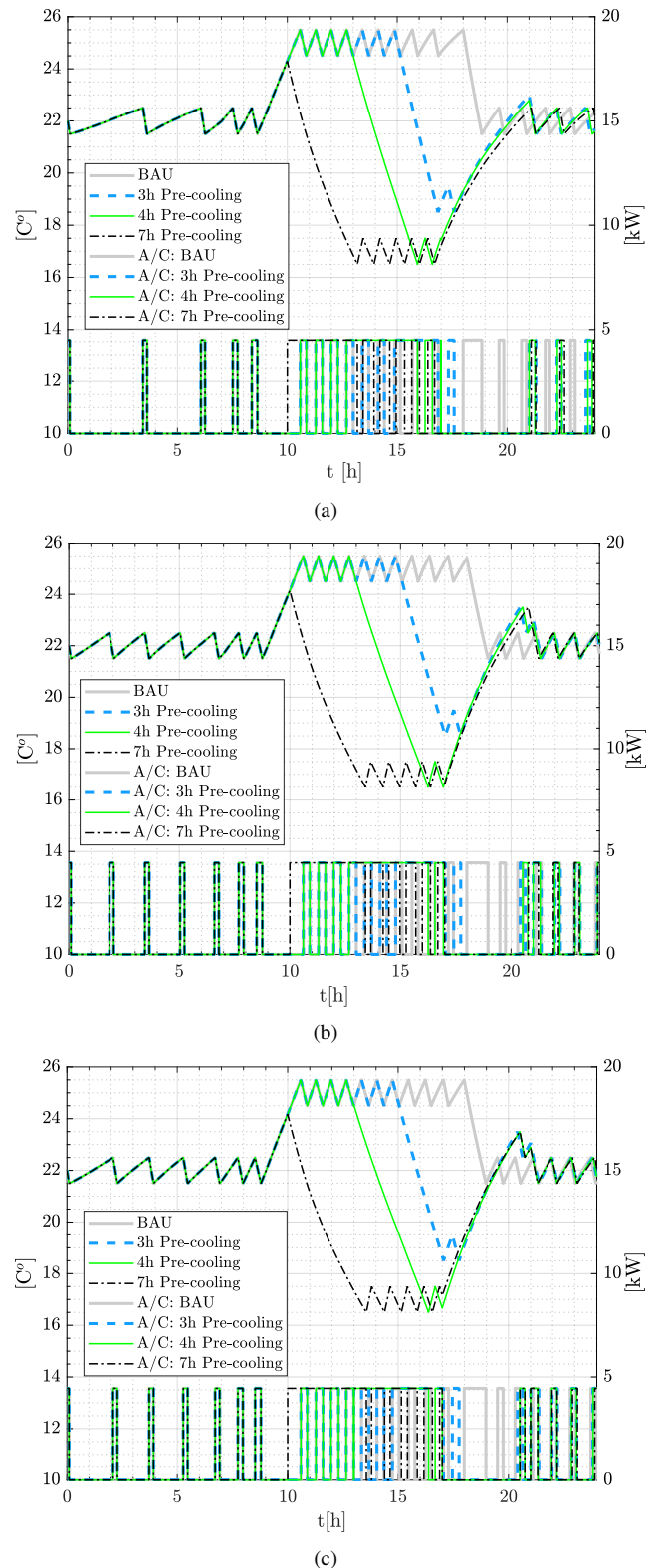


Fig. 12. Room 1 temperature and A/C operation for (a) Los Angeles, (b) Austin, and (c) Phoenix.

for Los Angeles and Austin, respectively, for the BAU ( $\tilde{d}^{\circ}$ ) and 7h pre-cooling ( $\tilde{f}^{\circ}$ ) cases. The other pre-cooling strategies were not considered, as their load shift was not sufficient for an effective duck-curve remediation, even worsening the

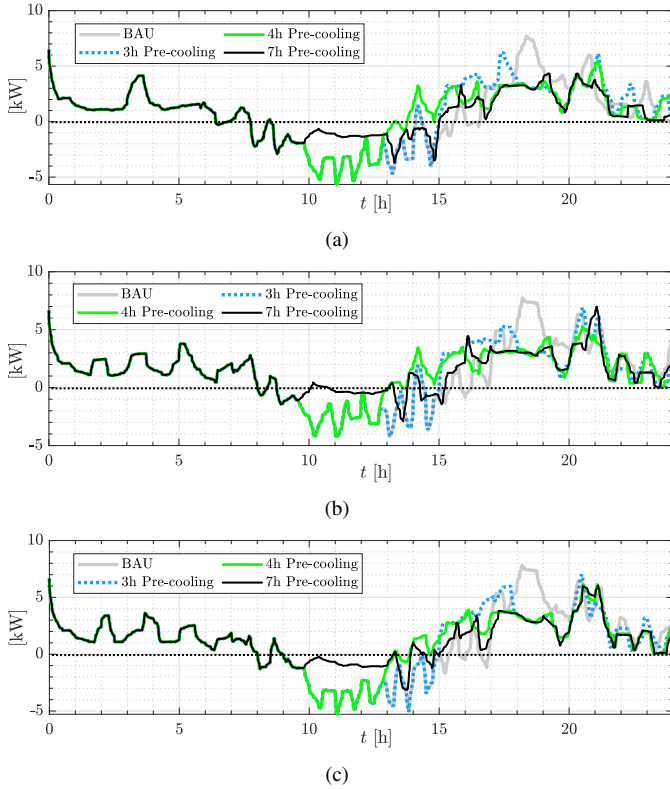


Fig. 13. Moving mean of house net demand for (a) Los Angeles, (b) Austin, and (c) Phoenix.

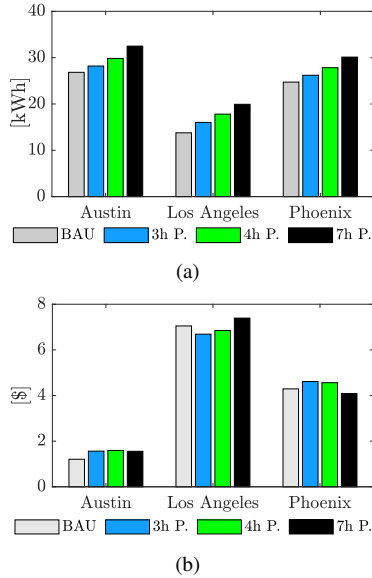


Fig. 14. Thermal simulation results: (a) net energy consumed, and (b) energy cost.

problem in some cases. The hourly system demand profiles for the aforementioned days were obtained from CAISO's and ERCOT's web sites. Since the PV installed capacity at the distribution level is around 10.4 GW in California and 0.99 GW in Texas [43], the PV generation profiles reported by CAISO and ERCOT for their bulk systems were scaled down to these values. Since the data resolution of  $d^\circ$  and  $f^\circ$  are fractions of an hour, three different values of  $\Delta t$  were

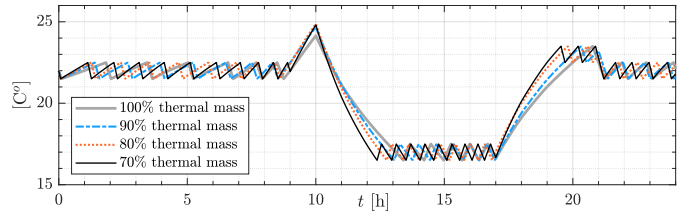


Fig. 15. Room 1 temperature in an Austin household for different thermal mass values and 7h pre-cooling.

considered in developing the aggregated models, i.e.,  $\Delta t = 1$  h,  $\Delta t = 0.5$  h, and  $\Delta t = 0.25$  h, which also required performing linear approximation between consecutive points to increase the resolution of the hourly system demand profiles to match the resolution of  $\tilde{d}^\circ$  and  $\tilde{f}^\circ$ , respectively. The model parameters are summarized in Table IV. The parameter values  $\Psi$  were obtained by trial and error, so that the the lowest prediction error was achieved for a relatively smooth curve.

The aggregated demand models for California and Texas, for  $\Delta t = 0.25$  h, are presented in Figs.16(a) and 16(b), respectively. Note that the models are accurate since they match the actual demand with the residential and base demand components showing shapes similar to typical system demands of their kind. The models using lower data resolution, i.e.,  $\Delta t = 0.5$  h and  $\Delta t = 1$  h, resulted in similar accuracy.

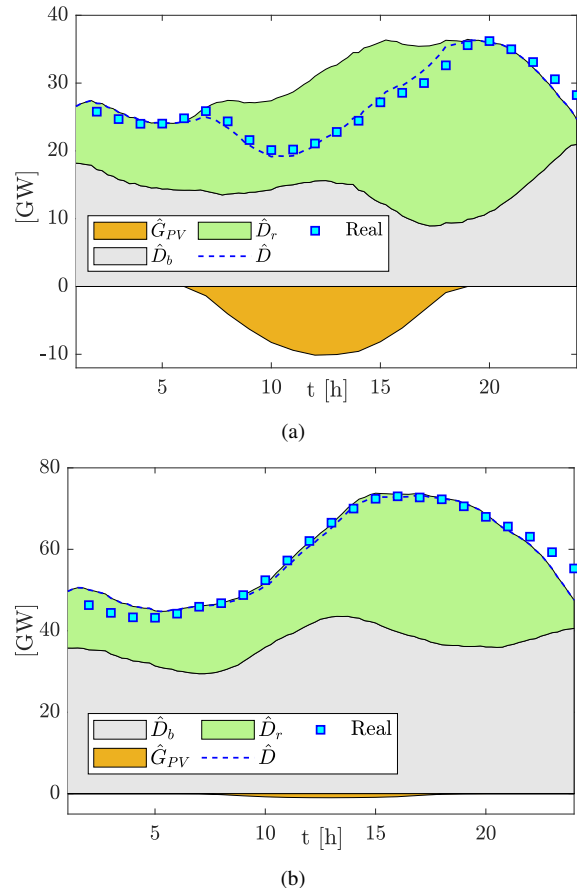


Fig. 16. Net demand model for  $\Delta t=0.25$ h for (a) California and (b) Texas.

TABLE IV  
AGGREGATED MODEL PARAMETERS.

System	$\Psi$	$H_o$	$\chi$	$\alpha_o$	$\sigma_{\max}$
California	$0.04/\Delta t$	$14e+6$	0.7	0.1236	2
Texas	$0.05/\Delta t$	$9.787e+6$	0.7	0.02	2

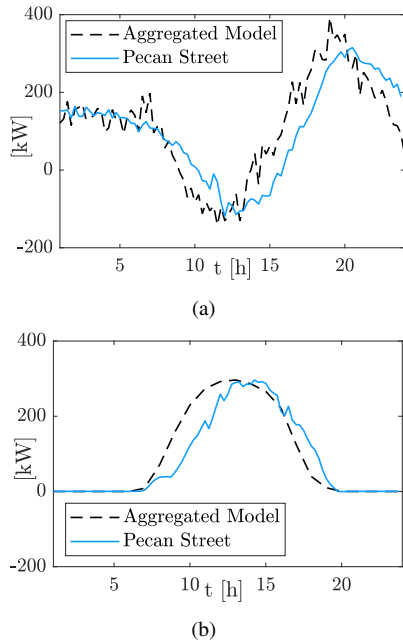


Fig. 17. Comparison between simulated and actual (a) net load and (b) PV injections for a reference neighborhood in Austin, TX.

The impact of different PV penetration levels and adoption levels of the 7h pre-cooling strategy on the net demand of California and Texas, is presented in Figs. 19 and 20, respectively, for data resolutions of  $\Delta t = 0.25$  h,  $\Delta t = 0.5$  h and  $\Delta t = 1$  h. The adoption levels range from  $\beta = 0$  (BAU in all houses) to  $\beta = 0.5$  (7h pre-cooling in 50% of houses), for PV penetrations of  $\alpha_o$ , and  $2\alpha_o$  (twice the current capacity) in California, and for  $\alpha_o$  and  $20\alpha_o$  in Texas, since the latter has relatively low penetration of installed PV units currently (Table IV).

1) *Model Validation*: To validate the proposed methodology, the net residential demand component of the Texas model is compared in Fig. 17 with data from an Austin's neighborhood of 83 households with significant installed PV capacity [44], for a summer day (August 16, 2018) with similar weather conditions as those considered for Texas. The average net energy consumed by a house in this community in the day studied is 31.16 kWh, while the average for a household in the BAU case is 31.23 kWh. Observe that the model follows closely the main trend of the actual data, in which the relatively small differences can be attributed, for the most part, to different PV injection profiles.

2) *California Case*: Observe in Figs. 19(a)-(c) that increasing adoption of 7h pre-cooling increases the net demand during the valley hours and reduces the system peak demand, which tends to flatten the system demand curve. As a result, the ramping generation requirement between 11:00 to 20:00 reduces

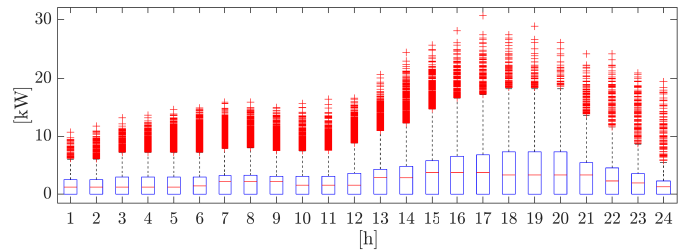


Fig. 18. Box plot of Texas' BAU aggregated residential demand.

significantly from 17 GW when  $\beta = 0$ , to approximately 4 GW when  $\beta=0.5$ . On the other hand, Figs. 19(d)-(f) demonstrate that doubling the penetration of residential PV units increases the ramping generation requirements to 26.6 GW when there is no pre-cooling ( $\beta = 0$ ), while a 50% of 7h pre-cooling adoption would be sufficient to bring the ramping generation requirements back to 2020's levels, i.e., about 18 GW. Finally, no significant differences are observed as the value of  $\Delta t$  varies, which demonstrates that the aggregation methodology is equally effective, regardless of the data resolution.

3) *Texas Case*: Due to the relatively low penetration of residential PV units in Texas, a duck shape is not observed in the system demand profile in Figs. 20(a)-(c). In such circumstances, adopting too much pre-cooling ( $\beta=0.5$ ) shifts the time of peak demand earlier, making it more challenging for the ISO, who must commit more reserves and dispatch more generation in a shorter period to guarantee a reliable supply, i.e., about 30.5 GW in less than 6 hours. However, if the PV penetration increases 20 times, as in Figs. 19(d)-(f), a duck-curve is formed, and then pre-cooling is shown to be effective in flattening the demand profile.

4) *Aggregated Load Characteristics*: In Fig. 18, a box plot summarizing the Texas' random BAU house load profiles, is presented. Note that the hourly house demand varies more from 15:00 to 21:00, suggesting that appliances such as A/Cs are operated differently from house to house, with larger variation at peak hours. In particular, this implies that a variety of A/C schedules and thermostat set points resulting from the random generation of household load profiles are different from the benchmark (average) house demand profile, thus representing varied household consumptions and behaviours.

5) *Load Factor*: In order to quantify the combined effect of pre-cooling and PV penetration in the simulation results for California and Texas, the Load Factor ( $LF = \frac{1}{n} \sum (\hat{D}_i) / \max(\hat{D})$ ) is presented in Figs. 21(a) and (b), respectively. Observe that increasing the pre-cooling adoption in California improves the LF in all cases, by around 0.09. On the other hand, for the current PV penetration in Texas, pre-cooling does not significantly improve the LF; in fact, adoption levels larger than 10% would negatively impact the LF. However, similar behaviour to that in California is observed when the PV penetration in Texas increases significantly, i.e., for  $20\alpha_o$ , which represents around 20 GW of PV generation, yielding better LFs than California.

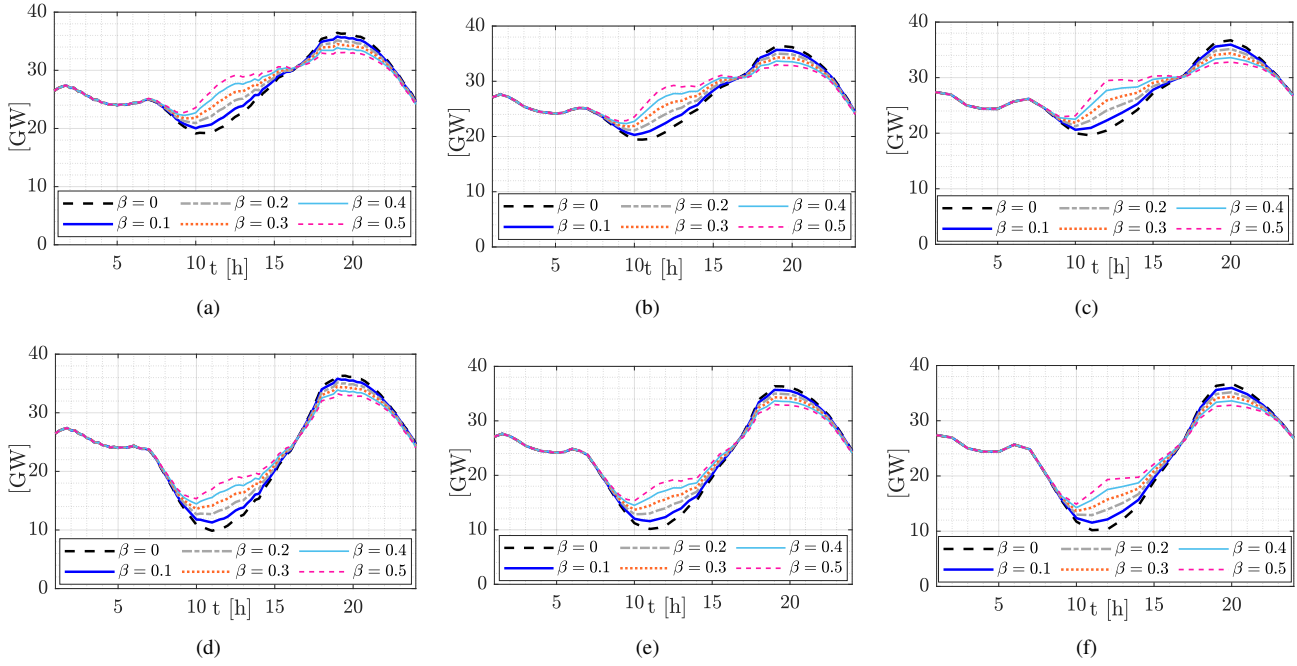


Fig. 19. Estimated net demand for California for  $\alpha_0$  and (a)  $\Delta t = 0.25$  h, (b)  $\Delta t = 0.5$  h, and (c)  $\Delta t = 1$  h; and  $2\alpha_0$  and (d)  $\Delta t = 0.25$  h, (e)  $\Delta t = 0.5$  h, and (f)  $\Delta t = 1$  h.

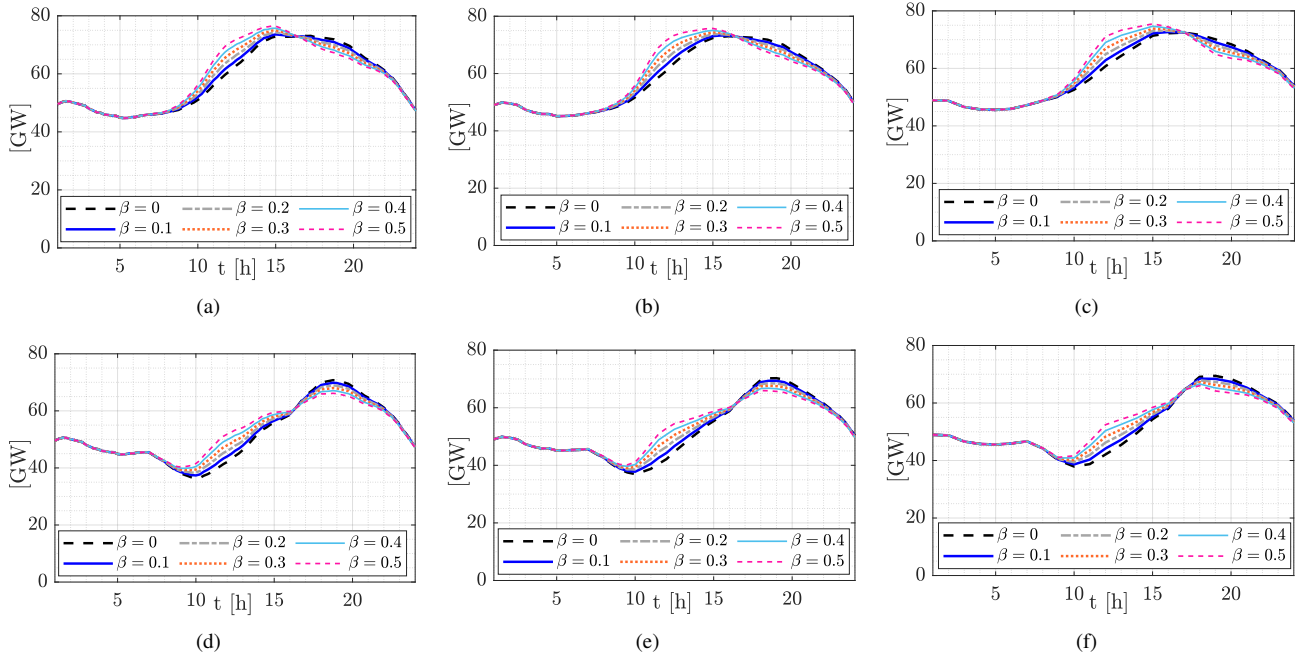


Fig. 20. Estimated net demand for Texas for  $\alpha_0$  and (a)  $\Delta t = 0.25$  h, (b)  $\Delta t = 0.5$  h, and (c)  $\Delta t = 1$  h; and  $2\alpha_0$  and (d)  $\Delta t = 0.25$  h, (e)  $\Delta t = 0.5$  h, and (f)  $\Delta t = 1$  h.

V. CONCLUSIONS

In this paper, the application of pre-cooling of residential customer households to address the system duck-curve issues was discussed, demonstrating through dynamic simulations that the thermal mass of a well-insulated North American house was large enough to allow longer pre-cooling, based on the ambient conditions of three US cities where deployment of small-scale PV is likely. Moreover, simulations of the aggregated household loads confirmed that long pre-cooling

could indeed address the issues of the existing California's duck curve, yielding acceptable LFs when the PV penetration increased by 50%, while in Texas, pre-cooling would be useful only when PV penetration levels were similar to California, with significant improvement in its LF. However, the feasibility of pre-cooling to address the duck-curve issue cannot be generalized, because the ambient conditions (temperature and solar irradiance), the availability of A/C in the households, and the typical thermal characteristics of the houses may

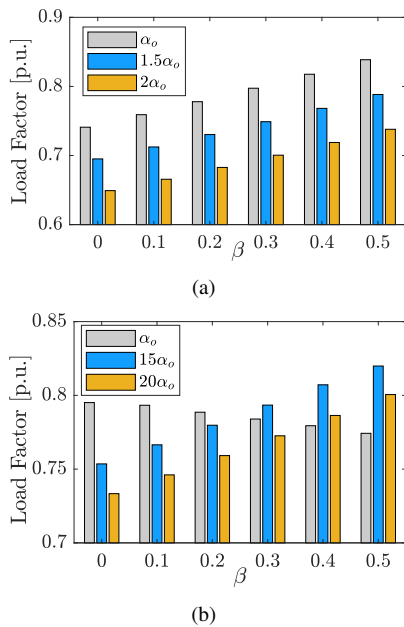


Fig. 21. Load Factor for different penetration levels of PV and adoption levels of pre-cooling in (a) California and (b) Texas.

significantly vary from one system to another. Nevertheless, the proposed methodology could be used to evaluate if a specific pre-cooling strategy would be effective for a given system, as demonstrated in the paper for Texas and California.

From the presented economic analysis based on existing ToU tariffs, it is evident that although some savings could be accrued in Los Angeles if long pre-cooling was adopted, additional incentives are necessary to motivate the customers to adopt this strategy to the levels necessary to influence the duck-curve. Future work may include exploring the use of smart thermostats such as Google NEST, which would allow more complex and optimized pre-cooling settings.

## REFERENCES

- [1] "International energy outlook 2019," Tech. Rep., U.S. Energy Inf. Admin., Washington, DC, Sep. 2019.
- [2] "Heating and cooling strategies in the clean energy transition: Outlooks and lessons from Canada's provinces and territories," Tech. Rep., U.S. Energy Inf. Admin., Washington, DC, May 2019.
- [3] "What the duck curve tells us about managing a green grid," Tech. Rep., CAISO, Folsom, CA, 2012.
- [4] X. Kou, Y. Du, F. Li, H. Pulgar-Painemal, H. Zandi, J. Dong, and M. M. Olama, "Model-based and data-driven HVAC control strategies for residential demand response," *IEEE Open Access Journal of Power and Energy*, vol. 8, pp. 186–197, 2021.
- [5] W. Tumin, M. M. Olama, and S. M. Djouadi, "Adaptive control for residential HVAC systems to support grid services," in *IEEE PES Innovative Smart Grid Technol. Conf. (ISGT)*, Washington, DC, Feb. 2021, pp. 01–05.
- [6] A. Taşçıkaraoğlu, N. G. Paterakis, O. Erdiñç, and J. P. S. Catalão, "Combining the flexibility from shared energy storage systems and DLC-based demand response of HVAC units for distribution system operation enhancement," *IEEE Trans. Sustainable Energy*, vol. 10, no. 1, pp. 137–148, 2019.
- [7] D. T. Vedullapalli, R. Hadidi, and B. Schroeder, "Combined HVAC and battery scheduling for demand response in a building," *IEEE Trans. Industry Applications*, vol. 55, no. 6, pp. 7008–7014, 2019.
- [8] O. Erdiñç, A. Taşçıkaraoğlu, N. G. Paterakis, Y. Eren, and J. P. S. Catalão, "End-user comfort oriented day-ahead planning for responsive residential HVAC demand aggregation considering weather forecasts," *IEEE Trans. Smart Grid*, vol. 8, no. 1, pp. 362–372, 2017.
- [9] A. German and M. Hoeschele, "Residential mechanical precooling," Tech. Rep., U.S. Department of Energy, 2014.
- [10] H. O. R. Howlader, M. M. Sediqi, A. M. Ibrahim, and T. Senjyu, "Optimal thermal unit commitment for solving duck curve problem by introducing CSP, PSH and demand response," *IEEE Access*, vol. 6, pp. 4834–4844, 2018.
- [11] P. Julianto, A. Soeprijanto, and Mardlijah, "Dynamic economic load dispatch by introducing compressed air energy storage for solving duck curve," in *Int. Seminar on Intell. Technol. Appl. (ISITIA)*, Surabaya, Indonesia, Jul. 2020, pp. 129–134.
- [12] L. A. Wong, V. K. Ramachandramurthy, S. L. Walker, and J. B. Ekanayake, "Optimal placement and sizing of battery energy storage system considering the duck curve phenomenon," *IEEE Access*, vol. 8, pp. 197 236–197 248, 2020.
- [13] S. S. Ahmad, F. S. Al-Ismail, A. A. Almehezia, and M. Khalid, "Model predictive control approach for optimal power dispatch and duck curve handling under high photovoltaic power penetration," *IEEE Access*, vol. 8, pp. 186 840–186 850, 2020.
- [14] R. Torabi, A. Gomes, and F. Morgado-Dias, "The duck curve characteristic and storage requirements for greening the island of porto santo," in *Energy Sustain. for Small Developing Econ. (ES2DE)*, Funchal, Portugal, Jul. 2018, pp. 1–7.
- [15] M. Sheha, K. Mohammadi, and K. Powell, "Solving the duck curve in a smart grid environment using a non-cooperative game theory and dynamic pricing profiles," *Energy Convers. Manage.*, vol. 220, p. 113102, 2020.
- [16] E. Omine, H. Hatta, and T. Ueno, "A proposal of demand response program for suppressing duck-curve's ramp rate with large penetration of photovoltaic generation systems," in *IEEE PES Innovative Smart Grid Techn. Conf. (ISGT)*, Washington, DC, Feb. 2019, pp. 1–5.
- [17] M. A. Rahman, I. Rahman, and N. Mohammad, "Implementing demand response in the residential energy system to solve duck curve problem," in *2nd Int. Conf. Adv. Inf. Commun. Technol. (ICAICT)*, Dhaka, Bangladesh, Nov. 2020, pp. 466–470.
- [18] R. Jovanovic, S. Bayhan, and I. S. Bayram, "A multiobjective analysis of the potential of scheduling electrical vehicle charging for flattening the duck curve," *J. Comput. Sci.*, vol. 48, p. 101262, 2021.
- [19] B. Kulkarni, D. Patil, and R. G. Suryavanshi, "IOT based PV assisted EV charging station for confronting duck curve," in *Int. Conf. Comput. Techn., Electron. Mech. Syst.*, Belgaum, India, Dec. 2018, pp. 36–39.
- [20] J. M. G. López *et al.*, "Smart residential load simulator for energy management in smart grids," *IEEE Trans. Ind. Electron.*, vol. 66, no. 2, pp. 1443–1452, 2019.
- [21] "South australian rooftop solar switched off in search for stability." [Online]. Available: <https://www.pv-magazine.com/2021/03/19/south-australian-rooftop-solar-switched-off-in-search-for-stability/>
- [22] "Renewables watch for operating day: Friday, August 28, 2020." Tech. Rep., CAISO, Folsom, CA, 2020.
- [23] SRLS (V2.4), University of Waterloo. [Online]. Available: <https://uwaterloo.ca/power-energy-systems-group/downloads/smart-residential-load-simulator-srls>
- [24] A. Molina, A. Gabaldon, J. Fuentes, and C. Alvarez, "Implementation and assessment of physically based electrical load models: application to direct load control residential programmes," *IEE Proc. Gener., Transmiss. Distribution*, vol. 150, no. 1, pp. 61–66, 2003.
- [25] "PVWatts@ calculator." [Online]. Available: <https://pvwatts.nrel.gov/>
- [26] E. Mathews, P. Richards, and C. Lombard, "A first-order thermal model for building design," *Energy and Buildings*, vol. 21, pp. 133–145, 1994.
- [27] J. L. Wright and A. G. McGowan, "Calculating the solar heat gain of window frames," *ASHRAE Trans.*, vol. 105, pp. 1011–1021, 1999.
- [28] S. Klein, "Calculation of the monthly-average transmittance-absorptance product," *Solar Energy*, vol. 23, no. 6, pp. 547–551, 1979.
- [29] R. Perez, P. Ineichen, R. Seals, J. Michalsky, and R. Stewart, "Modeling daylight availability and irradiance components from direct and global irradiance," *Solar Energy*, vol. 44, no. 5, pp. 271–289, 1990.
- [30] J. E. Hay and D. C. McKAY, "Estimating solar irradiance on inclined surfaces: a review and assessment of methodologies," *Int. J. Solar Energy*, vol. 3, no. 4-5, pp. 203–240, 1985.
- [31] P. Loutzenhiser, H. Manz, C. Felmann, P. Strachan, T. Frank, and G. Maxwell, "Empirical validation of models to compute solar irradiance on inclined surfaces for building energy simulation," *Solar Energy*, vol. 81, no. 2, pp. 254–267, 2007.
- [32] R. De Dear, "Recent enhancements to the adaptive comfort standard in ashrae 55-2010," in *Proc. 45th Ann. Conf. Architectural Sci. Assoc.*, Sydney, Australia, Nov. 2011, pp. 16–19.

- [33] H. Taha, D. J. Sailor, and H. Akbari, "High-albedo materials for reducing building cooling energy use," Tech. Rep. DE93 001574, Lawrence Berkeley Laboratory, University of California, Berkeley, CA, Jan. 1992.
- [34] M. Redmond and A. Mastropietro, "Thermophysical and optical properties of materials considered for use on the ldsd test vehicle," in *45th Int. Conf. Environ. Syst.*, Bellevue, WW, Jul. 2015.
- [35] "NFRC energy performance label," Brochure, National Fenestration Rating Council, Greenbelt, MD, [Online]. Available: <http://www.nfrc.org>
- [36] "Residential building codes," Texas state law library, Austin, TX, 2021. [Online]. Available: <https://www.sll.texas.gov/law-legislation/texas/building-codes/residential-building-codes/>
- [37] "Building energy efficiency standards for residential and nonresidential buildings," California Energy Commission, Sacramento, CA, 2019.
- [38] "Phoenix building construction code (PBCC)," Phoenix City Council, Phoenix, AZ, 2018.
- [39] I. Richardson, M. Thomson, and D. Infield, "A high-resolution domestic building occupancy model for energy demand simulations," *Energy and Buildings*, vol. 40, no. 8, pp. 1560–1566, 2008.
- [40] Southern California Edison. [Online]. Available: <https://www.pec.coop/your-service/our-rates/rates-pricing/time-of-use/>
- [41] Pedernales Electric Cooperative. [Online]. Available: <https://www.pec.coop/your-service/our-rates/rates-pricing/time-of-use/>
- [42] Salt River Projec. [Online]. Available: <https://www.pec.coop>
- [43] "Electric power monthly with data for november 2020," Tech. Rep., U.S. Energy Inf. Admin., Washington, DC, Jan. 2021.
- [44] "Households data set," Pecan Street Inc., Austin, TX, 2021. [Online]. Available: <https://www.pecanstreet.org/dataport/>



**Ross Baldick** is Professor Emeritus in the Department of Electrical and Computer Engineering at The University of Texas at Austin. He has undergraduate degrees from the University of Sydney, Australia, and graduate degrees from the University of California, Berkeley. Dr. Baldick is a Fellow of the IEEE and the recipient of the 2015 IEEE PES Outstanding Power Engineering Educator Award.



**Ivan Calero** (S'17, M'21) received the diploma in electrical engineering from Escuela Politécnica Nacional (EPN), Quito, Ecuador, in 2008, and the Ph.D. degree in electrical and computer engineering from the University of Waterloo, Waterloo, ON, Canada, in 2020. From 2009 to 2010, he was with the National Electricity Council of Ecuador. His research interests include modeling, analysis and control of power systems.



**Claudio A. Cañizares** (S'85, M'91, SM'00, F'07) is a University Professor and Hydro One Endowed Chair at the ECE Department of the University of Waterloo, where he has been since 1993. His highly cited research focuses on modeling, simulation, computation, stability, control, and optimization of power and energy systems. He is the IEEE Trans. Smart Grid EIC; a Fellow of the IEEE, the Royal Society of Canada, and the Canadian Academy of Engineering; and is the recipient of the 2017 IEEE PES Outstanding Power Engineering Educator

Award, the 2016 IEEE Canada Electric Power Medal, and of multiple awards and recognitions from PES Technical Committees..



**Kankar Bhattacharya** (M'95, SM'01, F'17) received the Ph.D. degree in electrical engineering from the Indian Institute of Technology, New Delhi, India, in 1993. He was with the Faculty of Indira Gandhi Institute of Development Research, Mumbai, India, from 1993 to 1998, and with the Department of Electric Power Engineering, Chalmers University of Technology, Gothenburg, Sweden, from 1998 to 2002. In 2003, he joined the Electrical and Computer Engineering Department, University of Waterloo, Waterloo, ON, Canada, where he is currently a full

Professor. His current research interests include power system economics and operational aspects. He is a Registered Professional Engineer in the province of Ontario.